Mathematical Modeling and Kinetic Parameter Estimation in Batch Crystallization

P. Quintana-Hernández
Instituto Tecnológico de Celaya, Celaya, Guanajuato 38010, Mexico

E. Bolaños-Reynoso and B. Miranda-Castro
Instituto Tecnológico de Orizaba, Orizaba, Veracruz 94320, Mexico

L. Salcedo-Estrada
Universidad Michoacana de San Nicolás de Hidalgo, Morelia, Michoacán 58000, Mexico

DOI 10.1002/aic.10133
Published online in Wiley InterScience (www.interscience.wiley.com).

A dynamic model of a batch crystallizer was used to estimate the kinetic parameters in a sugar cane crystallization process. The mathematical model included mass, energy, and population balance differential equations, and empirical relationships (power-law–type) for nucleation, growth, and production–reduction rates. Experimental data were obtained from runs carried out at different agitation and cooling profiles. A nonlinear optimization process was used to fit 11 kinetic parameters to experimental data. The overall experimental error was estimated in 7.71% and the average asymptotic error of all kinetic parameters was less than 2%. The nucleation rate was favored by high agitation speed and natural cooling profiles. The maximum growth rate was reached when supersaturation was at a maximum. There was a no clear effect of agitation profiles on growth. The overall effect of the term production–reduction was in all cases positive, with the largest values found for natural cooling profiles. © 2004 American Institute of Chemical Engineers *AIChE J,* 50: 1407–1417, 2004
Keywords: crystallization, kinetic, modeling, optimization, sugar cane

Introduction

Crystallization is a solid–liquid separation process where mass is transferred from a solute dissolved in a liquid phase to a solid (crystal pure) phase. The crystallized solid particles form a homogeneous phase. At the industrial level, crystal products must have high purity, a specific crystal size distribution (CSD), and a desired crystal shape. Crystals with random CSD are not desired. To achieve a desired CSD it is important to control supersaturation through cooling temperature and agitation rate, among other factors. Crystals are formed when nuclei appear and then grow. In the cooling crystallization process, the kinetics of nucleation and crystal growth require supersaturation, which is obtained by a change in temperature. In continuous processes it is important to keep supersaturation at an optimum value that will yield a growth rate as high as possible and a low nucleation rate for a sufficiently coarse crystal product to be formed. This condition cannot be achieved in batch crystallization because supersaturation changes from the beginning to the end of the processing. Therefore, it is desirable to set a cooling profile that keeps supersaturation almost constant to prevent high nucleation rates and limits the number of new nuclei formed (Mersmann, 1995). On the other hand, agitation exerts an additional influence on CSD: low values induce agglomeration, aggregation, and flocculation of particles, whereas high values produce attrition and

Correspondence concerning this article should be addressed to P. Quintana-Hernández at pedro@iqcelaya.itc.mx.

breakage. Again, it is desirable to establish an agitation profile that increases mass transfer but reduces crystal destruction. A right combination of temperature and agitation profiles may induce optimal operation of batch crystallizers.

Cooling batch crystallization has been widely used because its operation is simple and experimental data are easily generated. Manipulated variables follow computer-based profiles (temperature, agitation) and response variables are read on-line (CSD, supersaturation, temperature). On the other hand, the modeling of batch crystallization is not simple. The full mechanistic model includes as independent variables time and three space dimensions, and it is not clear, thus far, what is the exact nature of the relationship between dependent and independent variables. Some attempts have been made to model crystallization. Randolph and Larson (1971) structured a model combining differential equations for mass and energy balances, partial differential equations for population balance, and algebraic equations for nucleation and growth kinetics. Miller (1993) proposed and solved a model for cooling batch crystallization using the numeric method of lines. Bolaños-Reynoso (2000) and Salcedo-Estrada (2000) modified Miller's model and included agglomeration and breakage. They evaluated kinetic parameters using nonlinear optimization techniques and experimental data obtained using different temperature and agitation profiles. Salcedo-Estrada et al. (2002) reported different models used in batch crystallization and the algorithms used for solving the set of equations.

Kinetic parameters can be determined in batch and in continuously operated crystallizers. Mixed-suspension mixed-production removal (MSMPR) crystallizers are the most commonly used continuously operated crystallizers. They are easy to operate and both the death rate and the birth rate—probably caused by attrition, breakage, agglomeration, and/or dissolution—may be controlled such that their influence on the final crystal size distribution becomes negligible. The MSMPR crystallizers are operated at steady state, the content is ideally mixed, and the volume of the solution is kept constant. Experiments are done at different residence times and kinetic parameters are estimated from direct relationships between volumetric hold-up, mean crystal size, and mean residence time. On the other hand, batch runs are more difficult to control but allow investigations to work over wider ranges of supersaturation. In general, batch runs are less time-consuming than MSMPR but require a more complex analysis because of the presence of experimental inaccuracies (death and birth of crystals). Kinetic parameters may be fitted from batch experimental data using nonlinear optimization (Stewart et al., 1992).

Sá et al. (1996) studied sucrose crystallization and compared an adsorption–integration model with an empirical power-law model. They found a significant variation in solution viscosity and, thus, in sucrose diffusivity. The results were better represented by the power-law equation, which did not give direct information about mass transfer mechanisms. The average exponent g for the power-law equation was 1.89, with a mean relative square error of 3% and 1.92 for the adsorption–integration model with a 3.64% error.

In this work, batch experiments were performed and the term "production–reduction" was added to the model to account for the experimental deviation from ideality. In addition, the size-independent growth rate and nucleation rate were evaluated as functions of the agitation rate. For simplicity, the production–reduction term was assumed as a power-law function of supersaturation, overall crystal mass, and agitation rate. No attempt to estimate individual effects of agglomeration, attrition, and breakage was done.

Mathematical Model

The population balance for a well-mixed constant volume batch cooling crystallizer, based on population density distribution $n(L)$ as a function of time, becomes

$$\frac{\partial(nV)}{\partial t} + V\frac{\partial(Gn)}{\partial L} = V[B^0 + \alpha(L)] \tag{1}$$

The $\alpha(L)$ term, called the production–reduction term, represents the birth and death rates generated by aggregation, agglomeration, crystal-crystal contact, crystal shaft contact, attrition, and breakage of crystals. Breakage and attrition are the result of mechanical and fluid dynamics operation conditions. They are not influenced at the beginning by the kinetics of crystallization. However, the small fragments produced may grow in a supersaturated solution. In general, it is difficult to formulate and measure the death and birth rates. In this work, an attempt to measure the global effect of death and birth of crystals is made using a power-law–type equation. Equation 2 shows the relationship of $\alpha(L)$ as function of a kinetic constant, supersaturation, total mass of crystals formed, and agitation. The overall effects of death and birth of crystals may be accounted as experimental deviations from an ideal batch operation

$$\alpha(L) = K_a S^a M_c^k N^r \tag{2}$$

The initial and boundary conditions for solving Eq. 1, as described by Farrell and Tsai (1994), are

$$n(L, 0) = n_0(L, 0) \tag{3}$$

$$n(0, t) = \frac{B^0}{G_{L0}} \tag{4}$$

The nucleation rate and the independent-size growth rate equations, expressed as power-law functions, include a power-law term to account for the effect of agitation, as recommended by Qiu and Rasmunson (1994):

$$B^0 = K_b S^b M_c^j N^p \tag{5}$$

$$G = K_g S^g N^q \tag{6}$$

The total mass of crystals formed is calculated as a function of the third moment

$$M_c = \rho_c K_v \mu_3(t) \tag{7}$$

in which the third moment is calculated as

$$\mu_3(t) = \int_0^\infty nL^3 dL \tag{8}$$

The overall mass balance and its initial condition become

$$\frac{dC}{dt} = -\rho_c K_v \frac{V}{M_w}\left[3\int_0^\infty GnL^2 dL + B^0 L_0^3\right] \tag{9}$$

$$C(0) = C_0 \tag{10}$$

The energy balances inside the crystallizer and in the cooling jacket, with their respective initial conditions, are given as follows:

$$\rho V C p \frac{dT}{dt} = -\Delta H_c \rho_c K_v V\left[3\int_0^\infty GnL^2 dL + B^0 L_0^3\right] - U_1 A_1 (T - T_w) \tag{11}$$

$$T(0) = T_0 \tag{12}$$

$$\rho_w C p_w V_w \frac{dT_w}{dt} = \rho_w F_{win} C p_w (T_{win} - T_w) + U_1 A_1 (T - T_w) + U_2 A_2 (T_{ex} - T_w) \tag{13}$$

$$T_w(0) = T_{w0} \tag{14}$$

The heat of crystallization is calculated as suggested by Fernández and Ballester (1974)

$$\Delta H_c = -12.2115 - 0.7937T \tag{15}$$

In summary, the model includes 11 kinetic parameters: K_b, b, j, p, K_g, g, q, K_a, a, k, and r that are estimated from experimental data.

Model solution

The method of lines (Tsuruoka and Randolph, 1987) was used to solve the model. The set of partial differential equations was transformed into a set of ordinary differential equations by means of discretization of spatial variables (Vemuri and Karplus, 1980). Equation 16 is applicable everywhere on the discrete grid except on the boundary and one place before the boundary limits

$$\frac{dn_{i,j+1}}{dt} = -G_j\left[\frac{n_{i-2,j} - 8n_{i-1,j} + 8n_{i+1,j} - n_{i+2,j}}{12\delta}\right] + \alpha(L)_j \tag{16}$$

where $\delta = L_{i+1} - L_i = \Delta L$.

For the boundary and one before the boundary limits, the calculations are made as follows:

$$\frac{\partial n_{0,j+1}}{\partial L} = \frac{-22n_{0,j} + 36n_{1,j} - 18n_{2,j} + 4n_{3,j}}{12\delta} + O(h^4) \tag{17}$$

$$\frac{\partial n_{1,j+1}}{\partial L} = \frac{-4n_{0,j} - 6n_{1,j} + 12n_{2,j} - 2n_{3,j}}{12\delta} + O(h^4) \tag{18}$$

$$\frac{\partial n_{L_{\max}-1,j+1}}{\partial L} = \frac{4n_{L,j} + 6n_{L-1,j} - 12n_{L-2j} + 2n_{L-3,j}}{12\delta} + O(h^4) \tag{19}$$

$$\frac{\partial n_{L_{\max},j+1}}{\partial L} = \frac{22n_{L,j} - 36n_{L-1,j} + 18n_{L-2,j} - 4n_{L-3,j}}{12\delta} + O(h^4) \tag{20}$$

Subscripts i refer to space coordinate and subscripts j to time coordinate. Crystal size distribution, temperature profiles, and solute concentration were determined experimentally. The set of algebraic–differential–integral equations was solved using an initial crystal size value of 15.1260 μm, increments of 20.2525 μm, and a final value of 2000 μm. The set of 101 ordinary differential equations was solved using a fourth-order Runge–Kutta.

Methodology

The experimental setup (Figure 1) consisted of a 2.5-dm^3 jacketed glass vessel (Pignat, Dn 159Bx-Trasiego VT 14) with four vertical evenly spaced wall baffles (to ensure a well-mixed suspension); an agitation motor of 0.37 kW (RW20DZM), with a three-blade impeller; a 16-dm^3 cooling tank (Huber HS40, -40 to $+150$°C), with an internal pump at a maximum flow rate of 18 dm^3/min; and two peristaltic pumps.

Three different cooling profiles were tested: natural, lineal, and cubic (Mayrhofer and Nyvlt, 1988). The initial temperature in all runs was 70°C. The natural cooling profile was obtained by introducing a step change of -30 ± 1°C in the cooling water flow rate. The linear and cubic profiles were obtained by manipulating both temperature and cooling water flow rate. A computer program controlled the progress of these profiles (Salcedo-Estrada et al., 2001). After the initial 30-min stirring period, agitation speed was either kept constant or varied from 600 to 50 rpm following different profiles (step, negative exponential, lineal, or cubic). The time for each run was set to 180 min. Testing all combinations among cooling and agitation profiles generated 15 different experiments, as shown in Table 1.

At the beginning of each run, a saturated solution was prepared by dissolving 2528 g of sugar cane crystals in 800 cm^3 of distilled water at 70°C (total solution volume of 2230 cm^3), as determined by Quintana-Hernandez et al. (2001). The mixture was agitated at 600 rpm for 30 min before the cooling process started. Table 2 shows the complete set of parameters used to solve the mathematical model.

Crystal size distribution was measured on-line with a MasterSizer S (Malvern Instruments Ltd., Worcestershire, UK). The particle size range, covered by the 300 mm lens used, was 0.5–880 μm. The MasterSizer S generated relative volume distributions on 98 size classes based on a logarithmic grid.

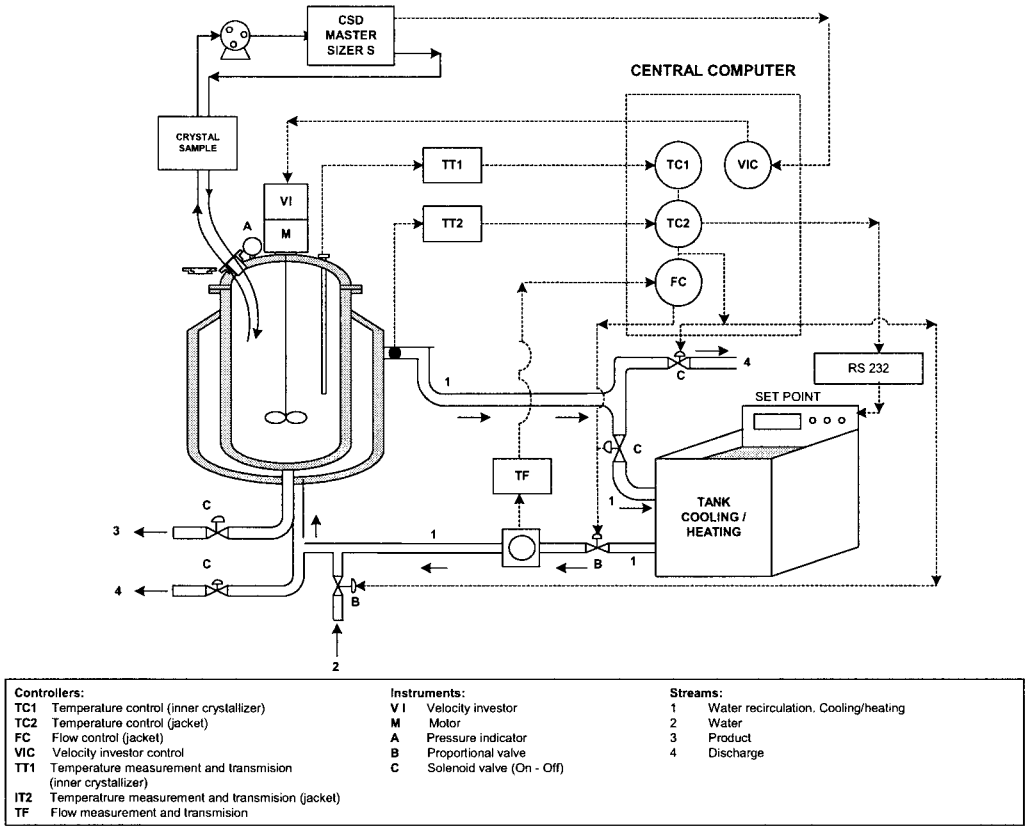

Figure 1. Batch crystallizer with integrated data acquisition system.

Quintana-Hernandez et al., (2000) determined the solution maximum flow rate that eliminated the destructive effects of measuring sugar cane crystals on-line. Reproducibility of measurements carried out with the MasterSizer S were confirmed using the standards provided by Malvern Instruments Ltd. The final product of each run was filtered and dried and its CSD was verified off-line. Solution concentration was measured with an Abbé refractometer (Atago USA, Kirkland, WA) every 10 min. Crystallizer and jacket temperatures were registered continuously as functions of time. Computer sampling and storing times varied at each run in the range of 5 to 12 min for CSD and from 1 to 3 min for temperatures.

Optimization

Kinetic parameter estimation was done with the GREG program (Stewart et al., 1987). A subroutine, MODEL, was implemented for nonlinear multivariable estimation. The parameter estimation was made based on the experimental data for CSD, temperature, and supersaturation as functions of time. GREG calculates derivatives using finite differences and minimizes a logarithmic sum of the determinant formed by the variance, $V^{(b)}$, among the estimated parameters θ. The optimization model becomes

Table 1. Experimental Design Followed to Generate Experimental Data

	Temperature Profiles		
Agitation Profiles	Natural	Linear	Cubic
Step	2	15	3
Negative exponential	9	14	7
Linear	10	8	4
Cubic	1	12	11
Constant at 600 rpm	6	13	5

Table 2. Process Parameters for Solving Mass, Energy, and Population Balances

Variable	Value	Units	Reference
Cp_s	2.4687	J/g °C	Quintana et al., 2001
K_v	$\pi/6$		Beckman, 1994
U_1	0.8354	J/°C · min · cm^2	Quintana et al., 2001
A_1	995.32	cm^2	Quintana et al., 2001
V	2230	cm^3	Bolaños, 2000
ρ_c	1.588	g/cm^3	Chen, 1991
T_0	70	°C	Bolaños, 2000
L_o	15.126	μm	Bolaños, 2000
ΔL	20.2525	μm	Bolaños, 2000
M_T	3328	g	Bolaños, 2000
M_w	800	g	Moncada and Rodríguez, 1999
M_s	2528	g	Moncada and Rodríguez, 1999
		Jacket	
Cp_w	4.18	J/g °C	Perry and Chilton, 1986
T_{wi}	70	°C	Bolaños, 2000
U_2	0.3236	J/°C · min · cm^2	Quintana et al., 2001
A_2	1334.88	cm^2	Quintana et al., 2001
F_{wi}	8100	cm^3/min	Bolaños, 2000
T_{ex}	29	°C	Bolaños, 2000
ρ_w	1.0	g/cm^3	Perry and Chilton, 1986
V_w	820	cm^3	Bolaños, 2000

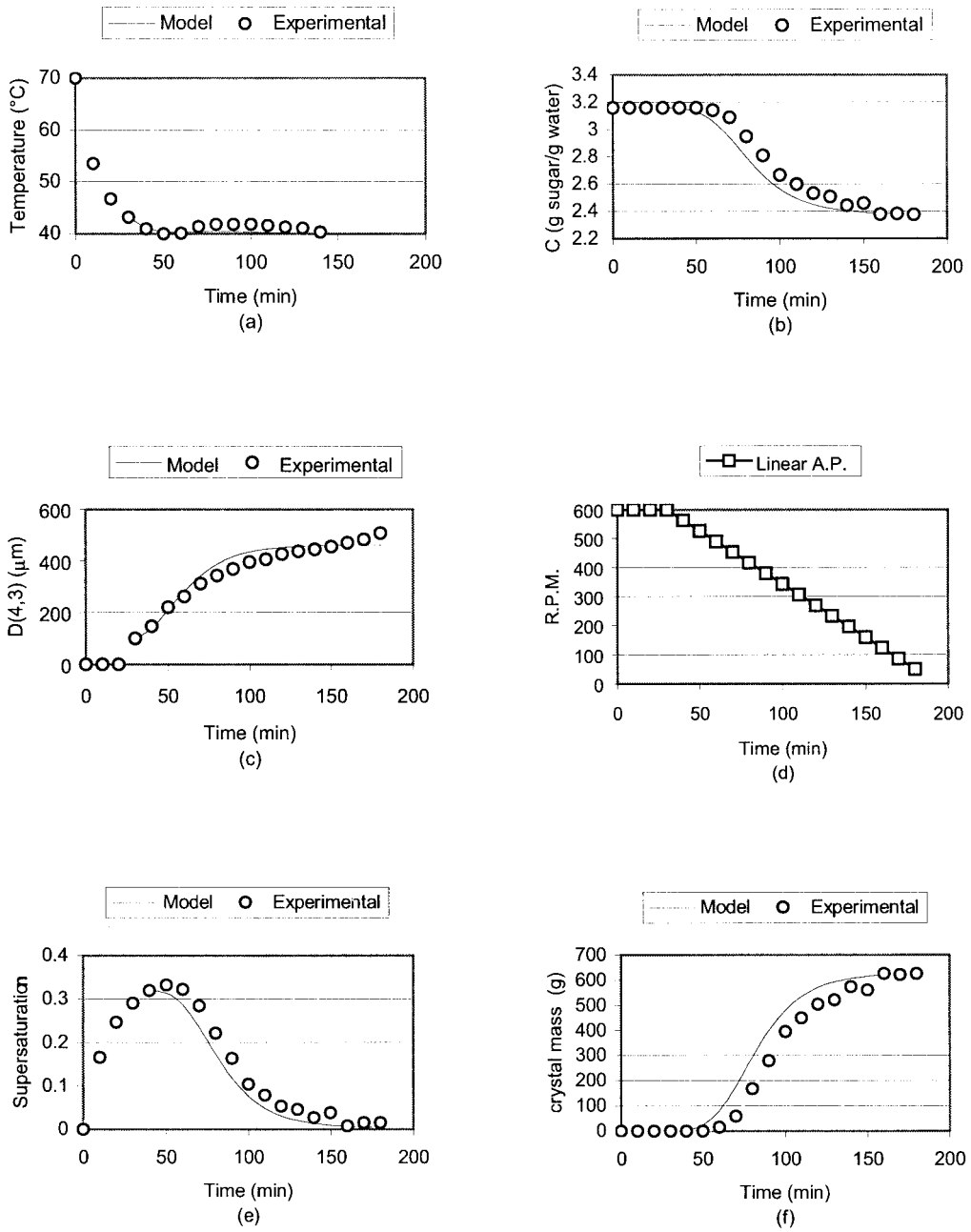

Figure 2. Experimental values and model approximation for run 10: (a) temperature profile, (b) concentration profile, (c) crystal average size *D*(4,3), (d) agitation profile, (e) supersaturation, and (f) crystal mass.

$$\min S = \sum_{b=1}^{Z} \ln|V^{(b)}(\theta)| \tag{21}$$

$$V_{ij}^{(b)}(\theta) = \sum_{ub} [\mathrm{OBS}(i,u) - F(i;u;\theta)][\mathrm{OBS}(j,u) - F(j,u;\theta)] \tag{22}$$

where OBS represents the experimental values, F the model values, and Z the number of experimental values times the optimization parameters.

The model solution values were compared with the experimental data to minimize the error and generate a new kinetic parameter vector with the estimated values. The iterative optimization process ends when the specified tolerance has been achieved.

Results and Discussion

Examples of experimental data and model calculations made with the estimated kinetic parameters are shown in Figures 2–4. Bolaños-Reynoso (2000) reported the complete set of experimental data. Experimental results confirmed that using a natural cooling profile generated a supersaturated sugar solution faster than other cooling profiles. The results of run 10

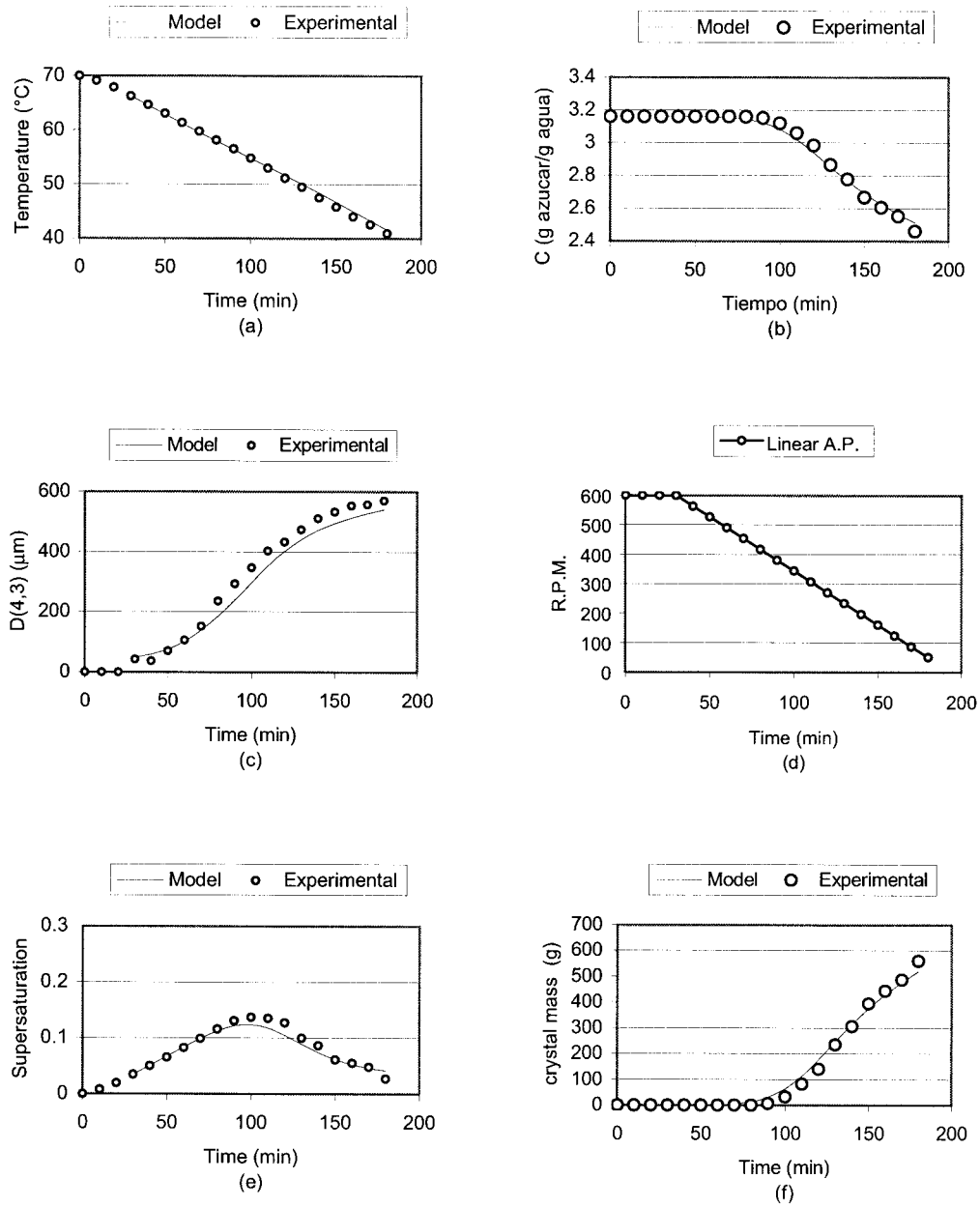

Figure 3. Experimental values and model approximation for run 8: (a) temperature profile, (b) concentration profile, (c) crystal average size *D*(4,3), (d) agitation profile, (e) supersaturation, and (f) crystal mass.

show that supersaturation reached a maximum at 50 min and decreased to a value close to zero at 180 min. At the end of this run the mass of crystals was 626 g, and the average crystal size was 507 μm with a standard deviation of 188 μm. For run 8 (linear cooling profile), supersaturation reached a maximum at 110 min. This value was smaller than the maximum obtained with the natural cooling profile. The mass of crystals at 180 min was 560 g and the average crystal size was 571 μm with a standard deviation of 201 μm. At the end of the run supersaturation had a value of 0.027. Runs made using cubic cooling profiles did not reach the expected final values after 180 min because supersaturation was kept at a very low value. For run 11, the mass of crystal formed in 180 min was 43 g and the average crystal size was 382 μm with a standard deviation of 156 μm. At the end of this run supersaturation was still increasing and had a value of 0.2863. For complete experiments with cubic cooling profile, the operation time must be greater than 180 min.

On the other hand, evaluation of the kinetic parameters showed that the nucleation rate constant K_b highly depends on cooling profiles and to a lower degree on agitation profiles. The largest value of K_b was obtained for run 6 using the natural cooling profile and constant agitation at 600 rpm, and the lowest value was for run 3 with the cubic cooling profile and negative step agitation profile. The nucleation exponent b had values between 0.001 and 0.035. This parameter did not present a clear dependency on either temperature or agitation rate. The crystal total mass exponent j presented lower values

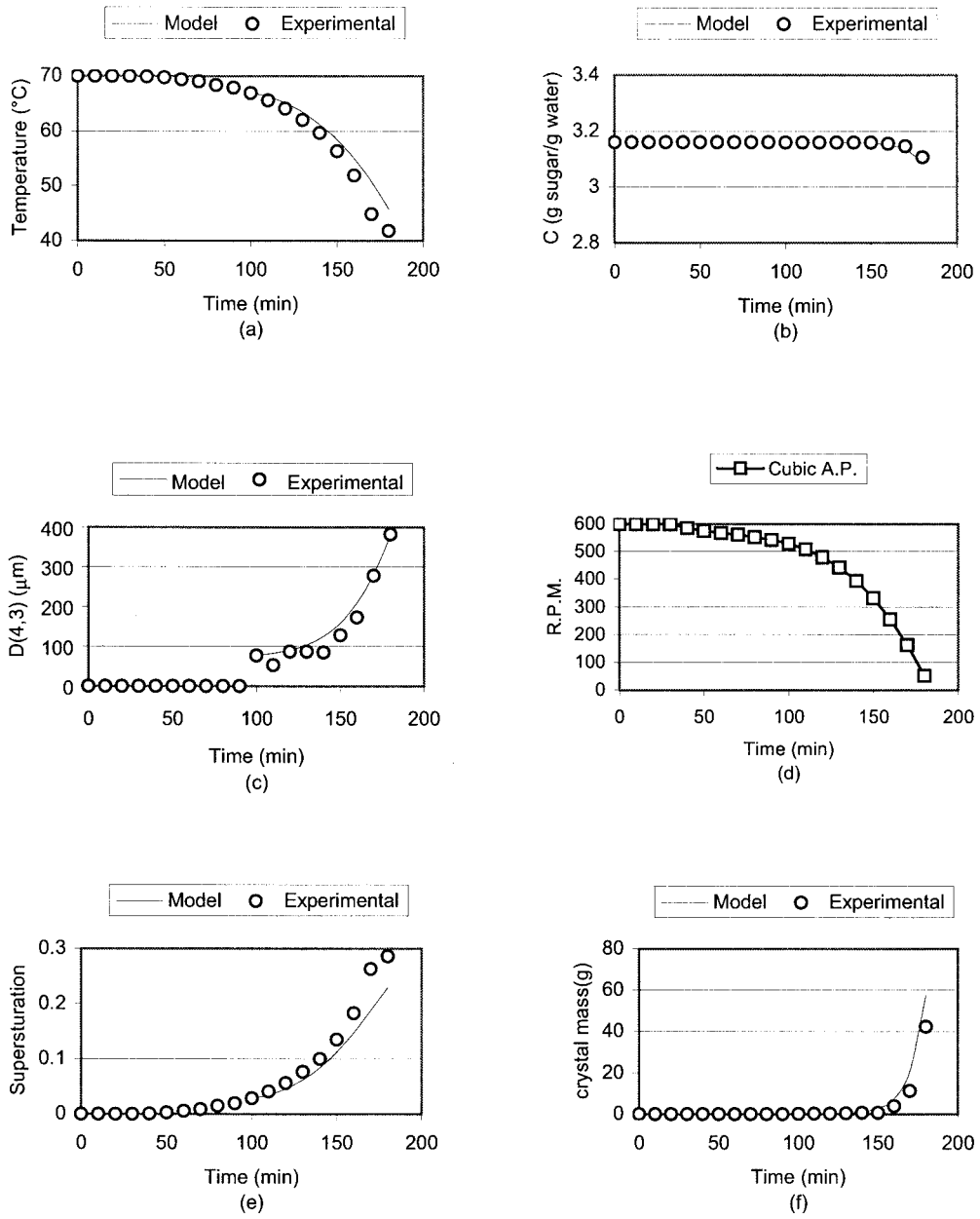

Figure 4. Experimental values and model approximation for run 11: (a) temperature profile, (b) concentration profile, (c) crystal average size *D*(4,3), (d) agitation profile, (e) supersaturation, and (f) crystal mass.

when natural cooling profiles were used because more crystals were formed with this cooling profile. This effect may indicate a low value of primary heterogeneous nucleation. The effects of parameter p, identified as the exponent of the agitation speed, was almost constant in all runs. The term N^p could be combined with the K_b in the analysis of nucleation. Figure 5 shows nucleation rates as a function of cooling and agitation profiles. It is clear that the K_b parameter has the greatest influence on nucleation rates and depends on the cooling profile. The analysis of different agitation profiles on nucleation rate showed that low values of agitation produced low values of nucleation at any cooling profile and high values of agitation increased the nucleation rate but following different patterns. The nucleation rate is highly favored by natural cooling profiles and linear, cubic, and constant agitation profiles.

The growth rate constant K_g presented different behaviors for each cooling profile. For a natural cooling profile, K_g decreased with agitation rate; for a linear cooling profile K_g increased with agitation speed; and for a cubic cooling profile K_g had a maximum for a negative exponential agitation profile. The supersaturation exponent for growth g is larger for natural cooling and presents interactions with the agitation speed. There is no clear pattern among agitation profiles and parameter g. The average value for g was 1.3. This value is smaller than that reported by Sá et al. (1996) because the model they used did not consider the effect of the mass of crystals formed

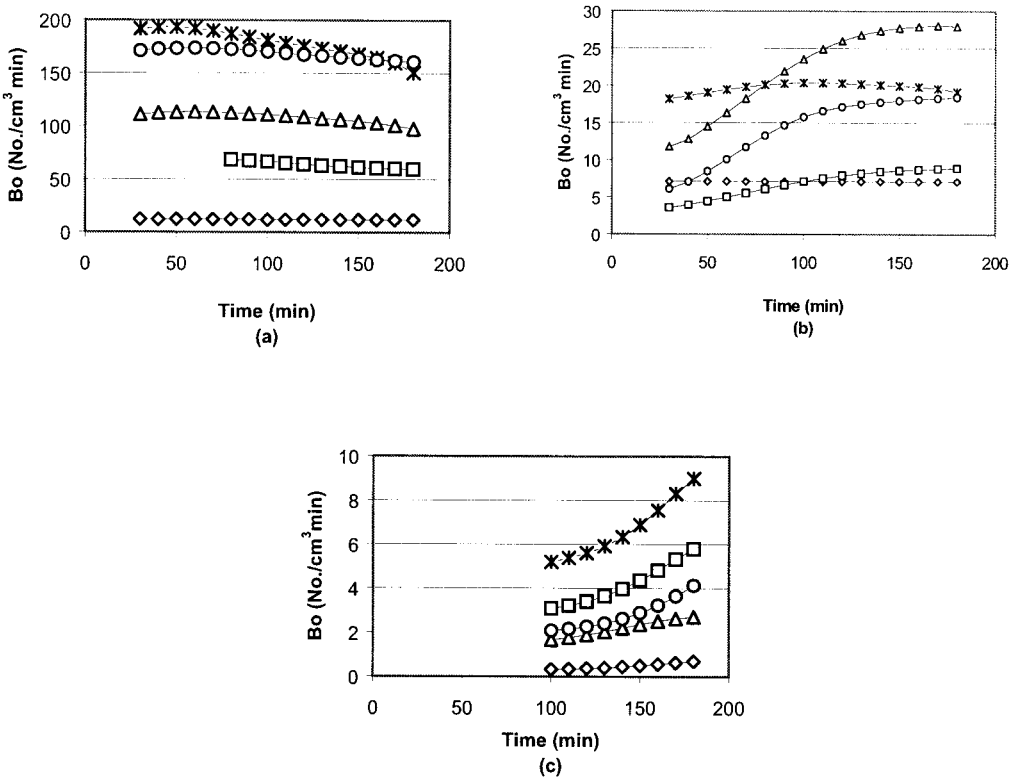

Figure 5. Nucleation rate as a function of cooling profiles: (a) natural, (b) linear, (c) cubic, and an agitation profile: ◇, step; □, negative exponential; △, linear; *, cubic; and ○, constant rate at 600 rpm.

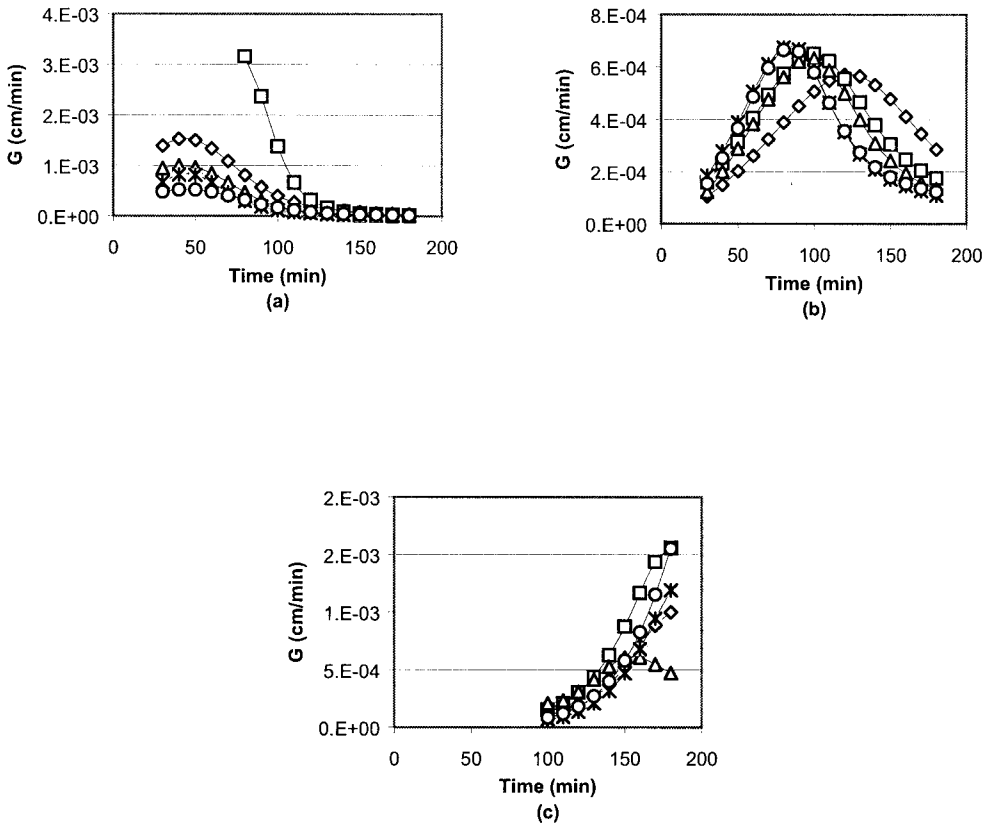

Figure 6. Grow rate as a function of cooling profiles: (a) natural, (b) linear, (c) cubic, and an agitation profile: ◇, step; □, negative exponential; △, linear; *, cubic; and ○, constant rate at 600 rpm.

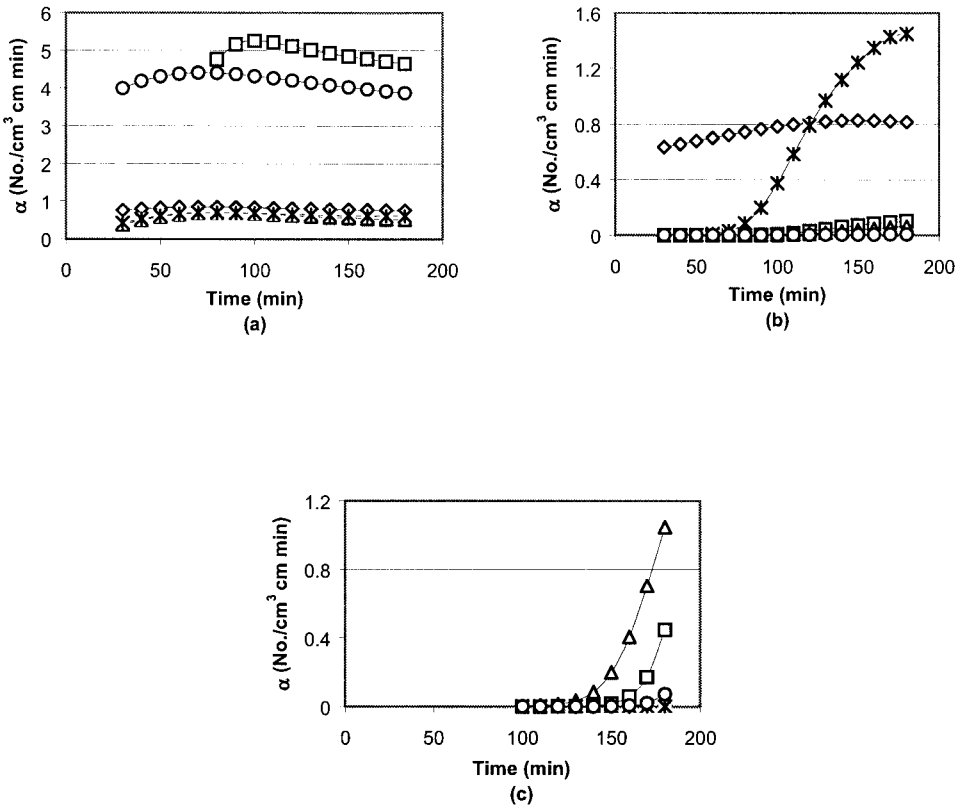

Figure 7. Production–reduction rate as a function of cooling profiles: (a) natural, (b) linear, (c) cubic, and an agitation profile: ◇, step; □, negative exponential; △, linear; *, cubic; and ○, constant rate at 600 rpm.

in their growth rate equation. The agitation rate exponent q has the greatest effect on natural cooling runs. Although the q values were close at each cooling profile, the value of the term N^q is 11.49 and 46.44 for runs 2 and 6, respectively. Figure 6 shows the growth rate as a function of cooling and agitation profiles. The growth rate exerted a substantial influence on supersaturation; maximum growth rates corresponded to maximum values of supersaturation. Agitation produced mixed effects depending of the cooling profile. Growth rates are favored by low agitation with natural cooling profiles and high agitation with linear and cubic cooling profiles.

The estimated parameters for production–reduction suggested interactions among the cooling and agitation profiles. Parameters for cubic cooling profiles were greater than those for natural and linear cooling profiles. In all cases the production rates were greater than the reduction rates (K_a was always positive) and the largest values were obtained for natural cooling profiles. The global effect of the production–reduction term is low compared to that of nucleation and growth terms. Figure 7 shows the production–reduction rates for different cooling and agitation profiles. There was no clear pattern of the production–reduction term as a function of cooling and agitation profiles.

B^0, G, and α were calculated for times greater than 30 min for natural and linear cooling profiles and for times greater than 100 min for cubic cooling profile because crystals were not detected by the MasterSizer before those times. Table 3 shows the estimated kinetic parameters for all 15 runs. The average asymptotic error of all kinetic parameters was less than 2%. The average error (model/experimental) for all 15 runs in the final crystal mass was 7.48%. The experimental error was estimated at 7.71%.

Conclusions

Experimental data were used to estimate kinetic parameters for the process of crystallization of sugar for different cooling and agitation profiles. The mathematical model was solved using the method of lines (discrete model) combined with a traditional fourth-order Runge–Kutta. The estimated kinetic parameters showed that the nucleation rate was favored by high agitation speed and natural cooling profiles. The maximum growth rate was reached when supersaturation was at a maximum. The overall effect of the term production–reduction was in all cases positive, with the largest values found for natural cooling profiles. The model with the estimated parameters was suitable to reproduce the experimental data within an experimental error of 7.71%. The average asymptotic error in the parameter estimation process was less than 2%.

Notation

A_1 = crystallizer's internal area, cm^2
A_2 = crystallizer's external area, cm^2
B^0 = nucleation rate, number of particles/cm^3·min
C = solute concentration, g of sugar/g of water
Cp = heat capacity of solution (magma), J/g·°C
F = flow rate, cm^3/min
G = size-independent crystal growth rate, cm/min

Table 3. Estimated Kinetics Parameters

Run	Nucleation (B^0)				Growing (G)			Production–Reduction (α)			
	K_b	b	j	p	K_g	g	q	K_a	a	k	r
Natural Cooling Profile											
2	10.50	5.03E-3	5.00E-4	3.50E-2	7.50E-4	1.50	6.24E-1	1.00	7.00E-2	2.50E-2	1.00E-3
9	61.36	3.50E-2	5.00E-4	3.50E-2	1.00E-3	1.41	6.36E-1	6.00	5.00E-2	2.50E-2	3.00E-3
10	85.70	1.00E-2	5.00E-3	5.00E-2	1.33E-4	1.00	5.00E-1	1.00	1.00E-1	9.00E-2	1.00E-3
1	150.00	5.00E-2	1.00E-3	5.00E-2	1.00E-4	1.50	6.12E-1	1.00	1.00E-1	9.00E-2	1.00E-3
6	159.97	3.00E-2	3.00E-3	2.00E-2	5.00E-5	1.30	6.00E-1	5.00	6.00E-2	2.01E-2	2.00E-3
Linear Cooling Profile											
15	7.00	1.00E-3	5.00E-5	3.50E-3	5.00E-4	1.222	6.08E-1	1.002	7.00E-2	2.50E-2	1.00E-3
14	10.00	5.01E-3	1.10E-1	1.50E-2	8.00E-3	1.299	5.00E-2	4.002	5.00E-1	1.50	2.00E-2
8	29.99	1.00E-3	1.00E-1	2.00E-2	7.00E-3	1.32	6.00E-2	1.014	1.01E-1	1.70	1.00E-2
12	20.00	2.97E-2	1.30E-2	2.00E-2	8.00E-3	1.308	8.00E-2	7.994	1.01E-1	1.10	5.00E-2
13	23.04	3.00E-2	1.30E-1	1.00E-2	1.10E-2	1.40	5.91E-2	1.00	8.00E-1	1.70	1.00E-2
Cubic Cooling Profile											
3	1.00	3.00E-2	1.30E-1	1.00E-2	7.16E-3	1.243	4.11E-2	1.371	7.63E-1	1.67	1.21E-2
7	7.00	1.00E-3	1.00E-1	2.00E-2	1.00E-2	1.203	6.00E-2	8.00	1.00E-1	1.10	5.00E-2
4	3.00	1.00E-3	1.00E-1	2.00E-2	9.70E-3	1.20	6.00E-2	8.00	1.00E-1	1.10	5.00E-2
11	12.00	1.00E-3	1.00E-1	2.00E-2	8.00E-3	1.40	4.00E-2	1.00	8.00E-1	1.70	1.00E-2
5	6.00	3.00E-2	1.04E-1	2.00E-2	7.01E-3	1.265	4.22E-2	8.00	1.00E-1	1.10	5.00E-2

K_a = kinetic coefficient for production–reduction, number of particles/cm^3 magma·cm^2·min·(g/cm^3)^k·(rpm)^r
K_b = kinetic coefficient for nucleation, number of particles/cm^3·min·(g/cm^3)^j·(rpm)^p
K_g = kinetic coefficient for growth, cm/min·(rpm)^q
K_v = crystal shape factor
L = crystal length, cm
M = mass, g
n = population density (number), number of particles/cm^3 slurry·cm
N = agitation rate, rpm
S = relative supersaturation
t = time, min
T = temperature of magma, °C
U_1 = heat transfer coefficient (magma–glass–water), J/°C·min·cm^2
U_2 = heat transfer coefficient (water–glass–air), J/°C·min·cm^2
V = magma volume, cm^3

Greek letters

$\alpha(L)$ = production–reduction rate, number of particles/cm^3 magma·cm·min
ΔH_c = crystallization enthalpy, J/g
ρ = magma density, g/cm^3
θ = estimated parameter vector

Subscripts and superscripts

a = production–reduction order
b = nucleation order
c = crystal
ex = exterior
g = growth order
i = size I
in = into the jacket
j = mass order at nucleation
k = mass order at production–reduction
p = agitation order at nucleation
q = agitation order at growth
r = agitation order at production–reduction
w = water

Acknowledgments

The authors acknowledge the financial support of Consejo Nacional de Ciencia y Tecnología (SEP–CONACyT), projects: 28142-U and J-37057-U; Consejo del Sistema Nacional de Educación Tecnológica (CoSNET), projects: 728.98 and 621.01-P; and Universidad Michoacana de San Nicolás de Hidalgo.

Literature Cited

Beckman, J. R., *Handbook of Chemical Engineering Calculations*, McGraw-Hill, New York (1994).
Bolaños-Reynoso, E., "Control y Optimización de las Condiciones de Operación de Cristalizadores Batch por Enfriamiento," PhD Dissertation, Instituto Tecnológico de Celaya, Mexico (2000).
Chen, J. C., *Manual del Azúcar de Caña*, Limusa, Mexico (1991).
Farrel, R., and Y. Tsai, "Modeling, Simulation and Kinetic Parameter Estimation in Batch Crystallization Processes," *AIChE J.*, **40**(4), 586 (1994).
Fernández, J., and L. Ballester, "The Heat of Crystallization and Activity Coefficients of Sucrose in Saturated Water Solutions," *Int. Sugar J.*, **2**, 40 (1974).
Mayrhofer, B., and J. Nyvlt, "Programmed Cooling of Batch Crystallizers," *Chem. Eng. Proc.*, **24**, 217 (1988).
Mersmann, A., *Crystallization Technology Handbook*, Marcel Dekker, New York (1995).
Miller, S. M., "Modelling and Quality Control Strategies for Batch Cooling Crystallizer," PhD Dissertation, University of Texas at Austin (1993).
Moncada-Abaunza, D., and O. Rodríguez-Cervantes, "Análisis de los Efectos de Agitación en la Unidad de Muestreo Durante la Determinación de Tamaño de Partícula," BS Thesis, Instituto Tecnológico de Celaya, Mexico (1999).
Perry, R. H., and C. H. Chilton, *Biblioteca del Ingeniero Químico*, McGraw-Hill, Mexico City, Mexico (1986).
Qiu, Y., and A. C. Rasmuson, "Estimation of Crystallization Kinetics from Batch Cooling Experiments," *AIChE J.*, **40**(5), 799 (1994).
Quintana-Hernández, P., R. Alfaro-Medina, E. Bolaños-Reynoso, and L. Salcedo-Estrada, "Efectos de Agitación en el Proceso de Cristalización," *Avances Ing. Quím.*, **8**(3), 73 (2000).
Quintana-Hernández, P., E. Bolaños-Reynoso, L. Salcedo-Estrada, and D. Moncada-Abaunza. "Determinación de Propiedades para Soluciones Saturadas de Azúcar," *Avances Ing. Quím.*, **9**(1), 43 (2001).
Randolph, A. D., and M. A. Larson, *Theory of Particulate Processes*, Academic Press, New York (1971).
Sá, S., L. Guimaraes, F. Rocha, and L. Bento, "Growth and Dissolution Kinetics of Sucrose Crystals," *Proc. 13th Int. Symp. Industrial Crystallization*, Tolouse, France (1996).
Salcedo-Estrada, L., "Control de Cristalizadores Tipo Batch," PhD Diss., Instituto Tecnológico de Celaya, Mexico (2000).

Salcedo-Estrada, L., P. Quintana-Hernández, and E. Bolaños-Reynoso, "Estrategia de Control para Cristalización por Lotes," *Rev. Ing. Quím.*, **20**, 34 (2001).
Salcedo-Estrada, L., P. Quintana-Hernández, and E. Bolaños-Reynoso, "Modelos Matemáticos en Cristalización por Lotes," *Rev. Ing. Quím.*, **21**, 3 (2002).
Stewart, W. E., M. Caracotsios, and J. P. Sorensen, *GREG: Manual del Usuario*, University of Wisconsin Press, Madison (1987).
Stewart, W. E., M. Caracotsios, and J. P. Sorensen, "Parameter Estimation from Multireponse Data," *AIChE J.*, **38**(5), 641 (1992).
Tsuruoka, S., and A. D. Randolph, "State Space Representation of the Dynamic Crystallizer Population Balance: Application to CSD Controller Design," *AIChE S. S. Crystall. Precip. Process.*, **83**, 104 (1987).
Vemuri, V., and W. Karplus, *Digital Computer Treatment of Partial Differential Equations*, Prentice Hall, Englewood Cliffs, NJ (1980).

Manuscript received Apr. 10, 2003, revision received Sept. 18, 2003, and final revision received Nov. 14, 2003.